Global Water Vapor Flux and Maintenance during FGGE

TSING-CHANG CHEN

Department of Earth Sciences, Iowa State University, Ames, IA 50011

(Manuscript received 1 December 1984, in final form 6 May 1985)

ABSTRACT

The relative humidity, temperature and wind fields generated by the First Global GARP Experiment (FGGE) III-b analysis of the Geophysical Fluid Dynamics Laboratory (GFDL) are used to examine the global precipitable water distribution, and the water vapor transport and maintenance for two extreme seasons of atmospheric circulation, i.e., December–February and June–August 1979.

It has been observed that the major water vapor content exists in tropical areas, especially over three regions: equatorial Africa, the northern part of South America, and equatorial western Pacific in December–February; equatorial Africa, Central America and the northern part of South America, and monsoon areas in June–August. The water vapor transport was analyzed to explore how the high water vapor content of these areas is maintained by the large-scale atmospheric circulation. It is concluded that 1) the nondivergent stationary mode describes most of the atmospheric water vapor transport; 2) the stationary divergent modes, mainly the local Hadley and Walker circulations, are responsible for the local maintenance of the high water vapor content over three tropical areas; and 3) the divergent transient modes, essentially the cyclone systems, transport poleward an important portion of water vapor along the storm tracks in midlatitudes of both hemispheres and two major cloud bands in the Southern Hemisphere.

1. Introduction

It has been three decades since the study of the moisture transport over North America was initiated by Benton and Estoque (1954) and over the Northern Hemisphere by Starr and White (1955). A subsequent series of studies of the hemispheric or global water vapor transport was made by Starr and his colleagues under the planetary circulation project (Starr and Saltzman, 1966) at the Massachusetts Institute of Technology (MIT). Research on this subject was carried on further by Starr's colleagues, including Rasmusson (1972), Rosen *et al.* (1979a), Peixoto *et al.* (1981), Salstein *et al.* (1980), and Peixoto and Oort (1983). The streamfunction (Rosen *et al.*, 1979b; Peixoto *et al.*, 1981) and potential function (Salstein *et al.*, 1980) of the water vapor flux were also employed to display the water vapor transport. Recently, Salstein *et al.* (1983) applied empirical orthogonal functions (EOF) to identify the most significant modes of the interannual variability of moisture flux. In addition to the MIT school, some efforts of other researchers were also devoted to the moisture transport. For example, Viswanadaham *et al.* (1980) used dew point depression to investigate the moisture condition of the Southern Hemisphere. Howarth (1983) also made an extensive computation of the water vapor transport over the Southern Hemisphere with data analyzed by the Australian World Meteorological Center.

There is no doubt that our understanding concerning water vapor transport in the atmosphere has been promoted and furthered tremendously in the last three decades through those studies. For instance, we have learned that the water vapor is concentrated in the tropics and decreases toward higher latitudes. The lower branch of the Hadley circulation transports moisture from subtropical to more tropical latitudes so as to maintain the gradient of precipitable water (e.g., Rasmusson, 1972). Moreover, the transient eddies effectively transport water vapor poleward to reduce the water vapor gradient (Starr and Peixoto, 1971). Nevertheless, the geographic distribution of precipitable water shows several areas of high water vapor content: the equatorial area of South America, monsoonal areas, and equatorial west Africa. Many studies cited here have focused on the moisture transport in the zonal and meridional direction, but only a few studies, e.g., Salstein *et al.* (1980), have attempted to seek the mechanism maintaining the high water vapor content geographically.

In reference to the local maintenance of water vapor content, Starr and Peixoto (1964) pointed out a dilemma indicating "when maps of the total eddy transport vector $\mathbf{Q}' = Q'_\lambda \mathbf{i}_\lambda + Q'_\phi \mathbf{j}$ are compared with the maps of precipitable water $\bar{W}$ (Starr *et al.*, 1958), it is evident that there is little correspondence between regions of mean eddy outflow and regions of high mean water vapor content." In fact, the same difficulty occurs when the total water vapor transport vectors are used.

Attempts were made by Starr *et al.* (1958, 1965) using the horizontal divergence (or convergence) of water vapor flux to explore the local maintenance of

water vapor content. Their conclusion does not shed much light on this matter because it is difficult to pinpoint the mechanisms responsible for the local maintenance of high water vapor content. Another approach is taken in the present study, namely, to examine the contributions to the water vapor flux from stationary (seasonal mean) and transient (departure from seasonal mean) modes. The separation of divergent and nondivergent modes is employed to isolate a particular type of atmospheric circulation which may be responsible for the local maintenance of high water vapor content.

Since the water vapor content essentially exists below 500 mb, a high resolution of the moisture field in the lower troposphere is desirable. The data generated by the First Global GARP Experiment (FGGE) III-b analyses of the Geophysical Fluid Dynamics Laboratory (GFDL) are used in this study. The purpose of this study is twofold: to provide the preliminary analysis of the water vapor flux using the GFDL FGGE III-b data and to gain a better understanding of the local maintenance of the atmospheric water vapor content. The data and formulation are discussed in Section 2. The precipitable water is described in Section 3, and the water vapor transport in Section 4. Section 5 examines the streamfunction and potential of the water vapor flux and the irrotational component of water vapor transport vectors, with concluding remarks in Section 6.

2. Data and analysis methodology

The data used in this study are the wind fields, relative humidity and temperature at mandatory levels of 1000, 950, 900, 850, 700, 500, 400, and 300 mb for 0000 and 1200 GMT generated by the GFDL FGGE III-b analyses (Miyakoda *et al.*, 1982; Ploshay *et al.*, 1983a,b). Based on comparison of the kinetic energy of the rotational and divergent wind at 200 mb between the European Center for Medium-Range Weather Forecasts (ECMWF) and GFDL FGGE III-b data, Julian (1984) cautioned that the GFDL analyses for the scales less than the planetary scales are much too creative, and often ignore the observed data. Rosen *et al.* (1984) also found that both the specific humidity and the transient eddy flux of moisture at 850 mb of the GFDL III-b analyses are noisy and have errors over some local areas. However, they pointed out that the general features of these two quantities are in agreement with other station based analyses.

At this point, we should note that an optimum interpolation scheme is applied to the GFDL data analyses which use the FGGE II-b data from various sources as the data base. During the data assimilation, the model solution is retained if there are no data at a grid point. The humidity data assimilated by the GFDL III-b analysis only come from rawinsonde stations plus some tropical wind observation system (TWOS) and drop windsondes.[1] Hence, the GFDL III-b moisture analyses over the tropics and the Southern Hemisphere may have model bias. On the other hand, Sirutis *et al.* (1980) demonstrated that a reasonable distribution of water vapor over the globe may be produced by inserting moisture data, even though fragmentary, into the GFDL model in the four-dimensional analysis. In addition, our preliminary comparison for the meridional transport of water vapor between the GFDL and ECMWF analyses shows that a significant meridional transport in the tropics exists in the former, but does not appear in the latter. Moreover, the water vapor content exists mainly in the lower troposphere below 500 mb. In addition to the data at the conventional mandatory levels, the GFDL analyses provide the relative humidity at 950 and 900 mb. For the preceding reasons, the GFDL FGGE III-b data were selected for the current study. The computations include the two extreme seasons of atmospheric circulation: December–February (DJF) and June–August (JJA). The specific humidity is evaluated by the Goff–Gratch (1946) formulation, which was applied in Chen *et al.* (1985).

The precipitable water in an air column is given by

$$\bar{W} = \frac{1}{g}\int_{P_u}^{P_L} \bar{q}\,d, \tag{1}$$

where g is the gravity, q is the specific humidity, and the overbar represents a time average over a season, i.e., stationary mode. The transient (departure from seasonal mean) mode of a given total variable ( ) is $(\ )' = (\ ) - (\bar{\ })$; P_u is 300 mb and P_L is usually 1000 mb. But the surface pressure is used as P_L for several regions. They are the Tibeta plateau, Rockies, Andes, and Antarctic where the surface pressure differs significantly from 1000 mb.

$$\bar{\mathbf{Q}} = \frac{1}{g}\int_{P_u}^{P_L} \overline{q\mathbf{v}}\,dp$$

$$= \frac{1}{g}\int_{P_u}^{P_L} \bar{q}\,\bar{\mathbf{v}}\,dp + \frac{1}{g}\int_{P_u}^{P_L} \overline{q'\mathbf{v}'}\,dp = \mathbf{Q} + Q', \tag{2}$$

where the total wind vector is $\mathbf{v} = u\hat{i} + v\hat{j}$. The $\mathbf{Q}$ and $\mathbf{Q}'$ denote the contributions by the stationary and transient mode, respectively. The zonal and meridional transport of water vapor are

$$\bar{Q}_\lambda = \frac{1}{g}\int_{P_u}^{P_L} \overline{qu}\,dp$$

$$= \frac{1}{g}\int_{P_u}^{P_L} \bar{q}\bar{u}\,dp + \frac{1}{g}\int_{P_u}^{P_L} \overline{q'u'}\,dp = \mathbf{Q}_\lambda + Q'_\lambda, \tag{3}$$

[1] Personal communication with Drs. R. D. Rosen and D. A. Salstein of Atmospheric and Environmental Research, Inc., and Dr. J. Ploshay of the GFDL.

and

$$\bar{Q}_\phi = \frac{1}{g}\int_{P_u}^{P_L} \overline{qv}\,dp = \frac{1}{g}\int_{P_u}^{P_L} \bar{q}\bar{v}\,dp + \frac{1}{g}\int_{P_u}^{P_L} \overline{q'v'}\,dp = \mathbf{Q}_\phi + Q'_\phi. \quad (4)$$

We may express the total water vapor transport as

$$\begin{aligned}\bar{\mathbf{Q}} &= \bar{Q}_\lambda \hat{i} + \bar{Q}_\phi \hat{j} \\ &= (\mathbf{Q}_\lambda \hat{i} + \mathbf{Q}_\phi \hat{j}) + (Q'_\lambda \hat{i} + Q'_\phi \hat{j}) \\ &= \mathbf{Q} + \mathbf{Q}'. \end{aligned} \quad (5)$$

Following Helmholtz theorem, we decompose the water vapor transport vector into the sum of its nondivergent (rotational) and divergent (irrotational) components in terms of the streamfunction (ψ) and potential (χ). Therefore,

$$\begin{aligned}\bar{\mathbf{Q}} &= \hat{k} \times \nabla\bar{\psi} + \nabla\bar{\chi} \\ &= \bar{\mathbf{Q}}_\psi + \bar{\mathbf{Q}}_\chi \\ &= (\hat{k} \times \nabla\psi + \nabla\chi) + (\hat{k} \times \nabla\psi' + \nabla\chi') \\ &= (\mathbf{Q}_\psi + \mathbf{Q}_\chi) + (\mathbf{Q}'_\psi + \mathbf{Q}'_\chi) \\ &= \mathbf{Q} + \mathbf{Q}'. \end{aligned} \quad (6)$$

Rosen *et al.* (1979) and Salstein (1980) used ψ and χ to display the water vapor transport and this approach is adopted here. The ψ and χ fields are obtained from

$$\nabla^2\psi = \hat{k}\cdot\nabla\times\mathbf{Q}, \quad \text{and} \quad \nabla^2\chi = \nabla\cdot\mathbf{Q}. \quad (7)$$

The numerical solutions of these Poisson equations are obtained in terms of the HWSSSP subroutine of the National Center for Atmospheric Research (NCAR) Software Subroutine Library; this subroutine was designed by Swarztrauber (1974). The boundary conditions of ψ and χ at both poles are specified such that the longitudinal gradient of ψ equals the normal flux and χ is zero.

3. Precipitable water content

The height–latitude distribution of the zonally averaged specific humidity ($\bar{q}$) (Fig. 1) shows that the water vapor content decreases toward the poles, similar to the zonally averaged temperature. The general feature of the $\bar{q}$ distribution is also similar to Rasmusson's (1972) result for the Northern Hemisphere and Peixoto and Oort's (1983) for the entire globe. It was pointed out by Trenberth (1981) that the Northern Hemisphere has a larger seasonal variation of water vapor content than the Southern Hemisphere. The latitudinal distribution of precipitable water ($\bar{W}$) depicted in Fig. 2 agrees with Trenberth's assessment. For example, $\bar{W}$ has a seasonal change from winter to summer of 8 kg m^{-2} at 30°S compared with 20 kg m^{-2} at 30°N.

Compared with the results of Howarth (1983) and

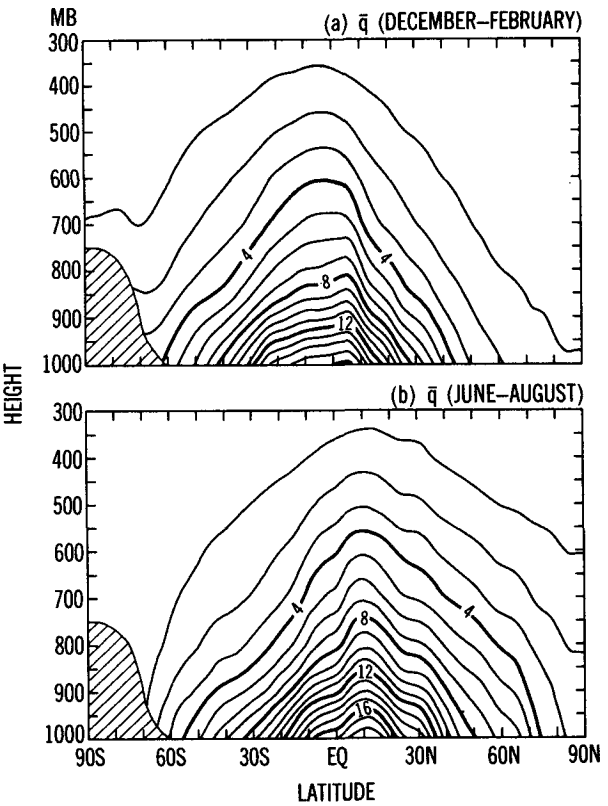

FIG. 1. Zonally averaged specific humidity ($\bar{q}$) for (a) December–February; (b) June–August. Units: gm kg^{-1}.

Peixoto and Oort (1983), the Southern Hemisphere $\bar{W}$ of the present study is somewhat smaller. For instance, $\bar{W}$ at 30°S in Fig. 2 is about 20% smaller than Howarth's $\bar{W}$ and about 10% smaller than Peixoto and Oort's $\bar{W}$. Howarth argued that his large $\bar{W}$ is attributed to the large mixing ratio at 1000 mb. On the other hand, the Northern Hemisphere $\bar{W}$ of this study agrees with the result of Peixoto *et al.* (1981) and Peixoto and Oort, with the exception of the summer maximum value of $\bar{W}$ at 10°N. In the tropics, our $\bar{W}$ is less than that of Peixoto *et al.* and of Peixoto and Oort during the northern winter (December–February). It is possible that such differences are linked to the weaker monsoon circulation during the FGGE northern winter (Greenfield and Krishnamurti, 1979).

Both Figs. 1 and 2 show that the largest water vapor content exists in the tropics. The zonal asymmetry of the $\bar{W}$ geographic distribution should occur essentially in these regions. According to the satellite observations of cloud coverage compiled by Sadler (1970) and the satellite inferred effective temperature analyzed by Liebman and Hartman (1982), intense convection is associated with the intertropical convergence zone (ITCZ), South Pacific Convergence Zone (SPCZ), and three tropical regions. These regions are the northern part of South America, equatorial Africa, and the

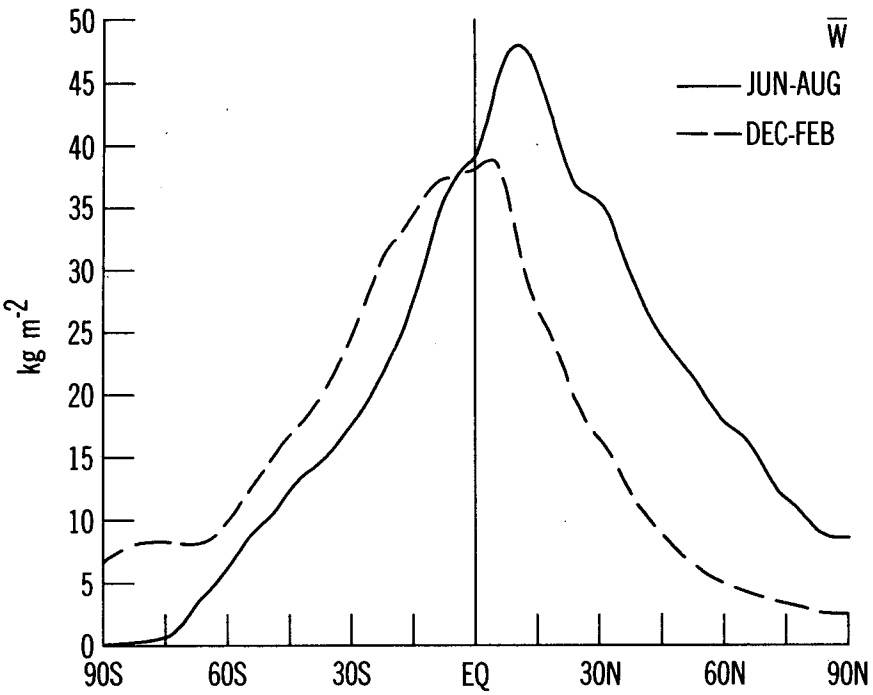

FIG. 2. Latitudinal distribution of zonally averaged precipitable water ($\bar{W}$) for December–February (dashed line) and June–August (solid line). Units: kg m^{-2}.

equatorial western Pacific during the northern winter (December–February), and Central America and the northern part of South America, equatorial west Africa, and monsoonal areas during the northern summer (June–August). A high water vapor content must exist over these areas to support the intense convection that occurs there. It is evident that the global distribution of $\bar{W}$ depicted in Fig. 3 for both the northern winter and summer support this assessment. As shown by the shading, regions of large $\bar{W}$ are observed to migrate between the two seasons. The largest values of $\bar{W}$ appear over the land areas in association with the higher temperature in the tropics. Furthermore, the seasonal change of temperature over the land masses is more significant than that over the ocean. The contrast of $\bar{W}$ between the northern winter and summer shown in Fig. 3 is consistent with the temperature variation. The conspicuous features of the $\bar{W}$ geographic distribution depicted above agree well with Peixoto and Oort's (1983) analysis.

In summary, the general distribution of $\bar{W}$ during the FGGE northern winter and summer is consistent with earlier studies. The minor discrepancies which exist are probably due to either the interannual variation, as Rosen *et al.* (1979) stated, and differences in the scheme of analysis, as Howarth (1983) stressed.

4. Water vapor transport

It was shown previously that water vapor essentially resides in the lower troposphere. Thus, the water vapor transport is vitally affected by the lower-level atmospheric circulation. Conventional studies usually employ geographic contour plots to illustrate the zonal and meridional transport of water vapor. To obtain a better view of how the water vapor transport is carried out by the low-level atmospheric circulation, as indicated by James and Anderson (1984), the geostrophic plots of the water vapor flux vector are displayed in Fig. 4. However, it might be somewhat difficult to verify results of the current study against earlier studies with the horizontal vector plots. Therefore, the height–latitude cross section and latitudinal distribution of various water vapor transports from our computations are applied.

a. Zonal transport

Figure 4a, d show that the zonal transport of water vapor, $[\overline{uq}]$,[2] occurs largely in the lower troposphere. The tropical easterlies cause the westward transport, and the midlatitude westerlies produce the eastward transport. A minor westward transport appears in the polar area. The overall $[\overline{uq}]$ distributions for both seasons in the current study are similar to Peixoto and Oort's (1983) result, except for the maximum westward transport of our $[\overline{uq}]$, which is found closer to the surface. Note that Peixoto and Oort's maximum $[\overline{uq}]$ is located near 800 mb in the Northern Hemisphere.

[2] [ ] = zonal mean.

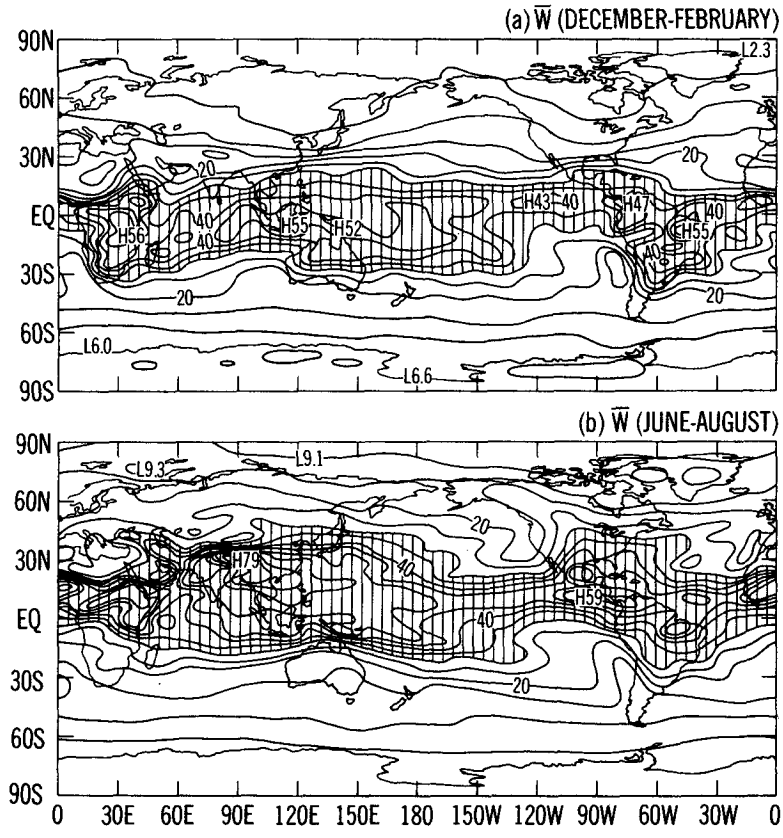

FIG. 3. Global distribution of precipitable water ($\bar{W}$) for: (a) December–February and (b) June–August. The areas with $\bar{W} \geq 30$ kg m^{-2} are shaded. Units: kg m^{-2}.

The latitudinal distribution of vertically integrated zonal transport of water vapor $\bar{Q}_\lambda$ is given in Fig. 5a. In the middle latitudes, Fig. 2 shows that the Northern Hemisphere has a larger difference of $\bar{W}$ between summer and winter. It is of interest to find in Fig. 5a that the maximum $\bar{Q}_\lambda$ of both summer and winter are comparable in the Northern Hemisphere. In the tropics, the maximum $\bar{Q}_\lambda$ migrates from the Northern Hemisphere tropics in December–February (northern winter) to the Southern Hemisphere tropics in June–August (northern summer). The disappearance of a maximum $\bar{Q}_\lambda$ in the Northern Hemisphere tropics from June–August is due to the strong westward transport of water vapor by the India monsoon and also the southward migration of trade winds. The contrast of maximum $\bar{Q}_\lambda$ values between the two seasons is consistent with Howarth (1983) for the Southern Hemisphere, Peixoto *et al.* (1981) for the Northern Hemisphere, and Peixoto and Oort (1983) for the entire globe both in magnitude and location.

The stationary mode $[\overline{uq}]$ is exhibited in Fig. 4b, e for the latitude–height cross section and in Fig. 5b for the latitudinal distributions of the vertically integrated $[\bar{u}\bar{q}]\mathbf{Q}_\lambda$. The remarkable similarity between $[\overline{uq}]$ and $[\bar{u}\bar{q}]$, and between Q_λ and $\mathbf{Q}_\lambda$ indicates that the zonal transport of water vapor is essentially carried out by the stationary mode. Note that the stationary mode $[\bar{u}\bar{q}]$ or $\mathbf{Q}_\lambda$ indicates contributions from both the time-mean zonal mean circulation and stationary eddies.

Peixoto *et al.* (1978) found that the transient zonal eddy transport of water vapor, $[\overline{u'q'}]$, is at least an order of magnitude smaller than $[\overline{uq}]$ or $[\bar{u}\bar{q}]$. From the latitude–height cross section (Fig. 4c, f) and the latitudinal distribution of vertical integral $[\overline{uq}]$ (Fig. 5c), it can be seen that the water vapor is transported westward by the transient mode in the tropics and high latitudes. The transport is eastward in the subtropics and mid-latitudes of both hemispheres. Since $[\overline{u'q'}]$ is equivalent to the difference of two large quantities, the error of this transport may be comparable to its magnitude. Therefore, any physical argument on this quantity should be treated with caution.

b. Meridional transport

The major meridional transport of water vapor, $[\overline{vq}]$, exhibited in Fig. 6a, d, occurs essentially in the layer below 700 mb. This transport in midlatitudes of both hemispheres (Fig. 7) is always poleward. In the tropics, $[\overline{vq}]$ follows the direction of the lower branch

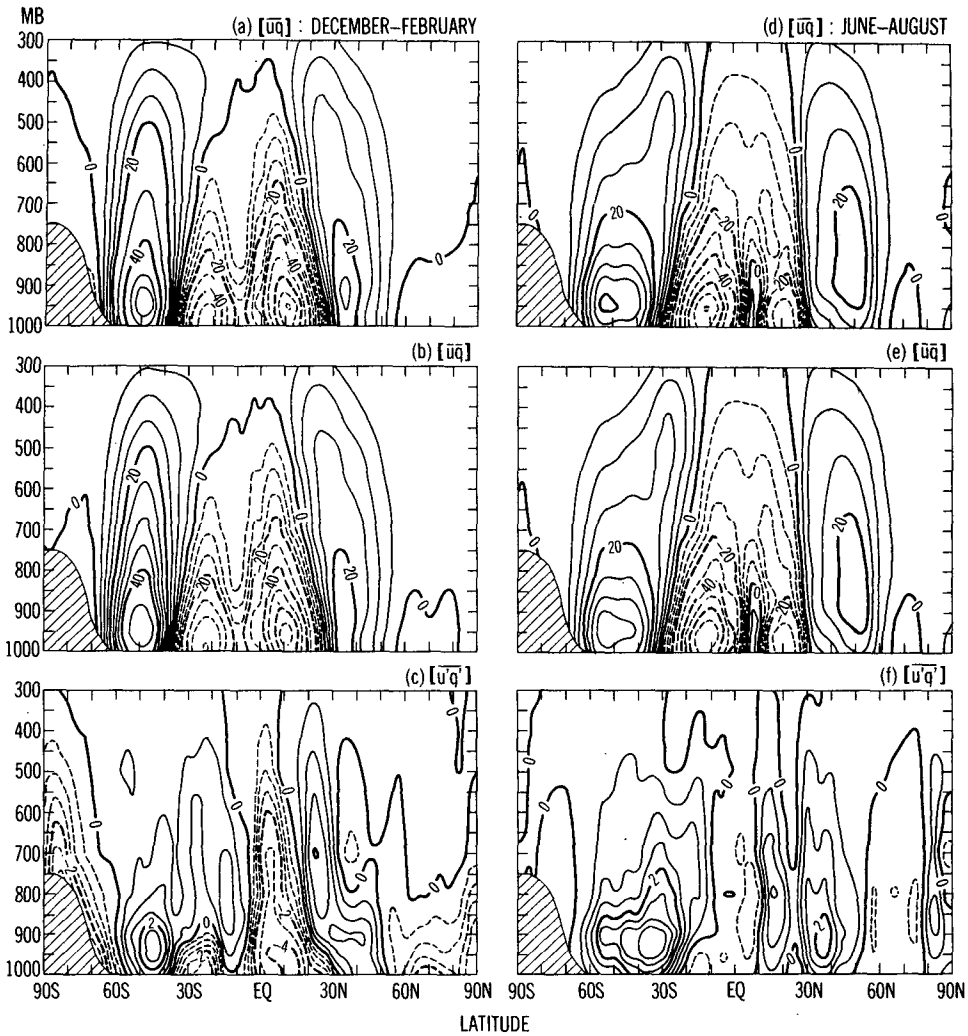

FIG. 4. Zonally averaged, zonal flux of water vapor performed by various modes of atmospheric circulation for two seasons: December–February and June–August. (a) and (d) are for total flow, (b) and (e) for the standing mode, and (c) and (f) for the transient-mode. The eastward and westward transports are designated by solid and dashed lines, respectively. Units: gm kg^{-1} m s^{-1}.

of Hadley circulation. For instance, the $\bar{Q}_\phi$ transport is northward from June through August and southward from December through February. Peixoto *et al.* (1981) and Peixoto and Oort (1983) showed that the maximum $\bar{Q}_\phi$ in the northern summer appears south of the equator and the minimum $\bar{Q}_\phi$ for the same season exists at 10°N. For this study, the maximum $\bar{Q}_\phi$ during the northern summer appears around the equator and the minimum $\bar{Q}_\phi$ exists at 20°N and 30°N with a minor maximum located between these two latitudes. In the northern winter, the maximum $\bar{Q}_\phi$ exists at 5°N which is about the same location as in the study of Peixoto *et al.* (1978). It is of interest to note that the maximum northward $\bar{Q}_\phi$ in summer is larger than the maximum southward $\bar{Q}_\phi$ in winter. A comparison of Howarth's (1983) Southern Hemisphere analyses of both seasons shows that his $\bar{Q}_\phi$ is much smaller which is probably due to an underestimate of meridional circulation in the Australian analysis.

The contribution of the stationary mode to the meridional transport $[\overline{vq}]$ (or $\mathbf{Q}_\phi$) indicates that the stationary mode describes most of the total meridional transport in the tropics. Note that the stationary mode includes the mean meridional circulation and stationary eddies. Rasmusson (1972) and Peixoto and Oort (1983) pointed out that the meridional water vapor transport by stationary eddies is significant only in the subtropics of the Northern Hemisphere during the summer. The minor maximum between 20° and 30°N in the current study is due to the stationary eddies (not shown).

The meridional water vapor transport by the transient mode shown in Fig. 6c, f for $[\overline{v'q'}]$ and Fig. 7c for Q'_ϕ becomes significant in midlatitudes and pole-

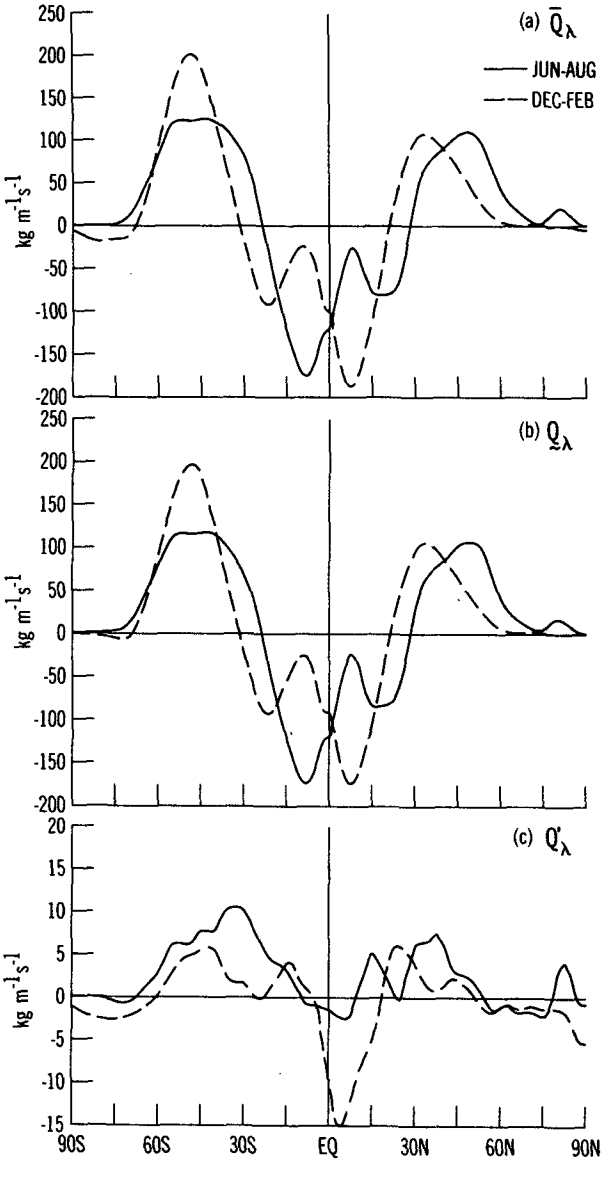

FIG. 5. Zonally averaged, vertically integrated zonal flux of water vapor for: (a) the total flow; (b) the standing mode; (c) the transient mode. December–February and June–August are denoted by dashed and solid lines, respectively.

ward in both hemispheres. Note that $[\overline{v'q'}]$ (or Q'_ϕ) contains contributions from both the transient eddies and the transient zonal mean meridional circulation. The latter is negligible in our analysis (not shown). In other words, $[\overline{v'q'}]$ is carried out chiefly by transient eddies which are active in midlatitudes.

Rasmusson (1972) stressed that the zonal mean meridional circulation tends to maintain the maximum water vapor content in the tropics, while transient eddies transport the water vapor out of this region. The poleward transport by transient eddies attains a maximum during winter and a minimum during summer. Rasmusson's assessment of the transient eddy transport of water vapor is consistent with the analyses for both hemispheres depicted in Figs. 6c, f, and 7c. Furthermore, $[\overline{v'q'}]$ is shown to be slightly larger in the Southern Hemisphere.

c. *Water vapor flux*

The global total water vapor transport during December–February (northern winter) (Fig. 8a) is dominated by the westward transport in the tropics due to the trade winds, the eastward transport in the midlatitudes around the entire Southern Hemisphere because of the westerlies, and the eastward transport along the jet streams of the Northern Hemisphere. Three anticyclonic cells of water vapor transport are evident over the Indian, Pacific, and Atlantic Oceans in the Southern Hemisphere. These are due to stationary oceanic anticyclones which act as buffers between the tropical trades and the midlatitude westerlies. During this season no significant anticyclonic transport cell is discernible over the oceans in the Northern Hemisphere. The water vapor is observed to converge toward the northern part of South America, the equatorial western Pacific and southern Africa. However, the large-scale circulation responsible for the convergence of water vapor flux toward these areas is not evident.

During the period of June–August (Fig. 9a), three anticyclonic cells of water vapor transport associated with the Pacific and Atlantic anticyclone, and Indian monsoon circulation become very pronounced in the Northern Hemisphere. Note that the strong northward transport along the east coasts of Asia and North America is due to strong wind fields, rather than a large water vapor content. In the Southern Hemisphere, an eastward transport between 30°–60°S is evident because of the strong midlatitude westerlies. Anticyclonic cells of water vapor transport with relatively strong intensity exist over the Pacific and Atlantic, while the anticyclonic cell over the Indian Ocean disappears during this season. Convergence of water vapor flux occurs in Central America and the northern part of South America and in monsoon areas; however, this phenomenon is not obvious over equatorial Africa. Note that the overall feature of the water vapor flux during this season is consistent with the analysis of James and Anderson (1984) using the ECMWF FGGE III-b data.

The vector distributions of the water vapor transport by the stationary mode $\mathbf{Q}$ for both seasons (Figs. 8b and 9b) are similar to those of $\bar{Q}$, especially in the tropics. On the other hand, the water vapor transport by the transient mode Q' for both seasons (Figs. 8c and 9c) exists largely in midlatitudes and is poleward in both hemispheres. In fact, the most significant areas of $\mathbf{Q}'$ in the Northern Hemisphere for both seasons coincide with "storm tracks" (Blackmon, 1977; Lau, 1978) which extend from the northeast Pacific to the

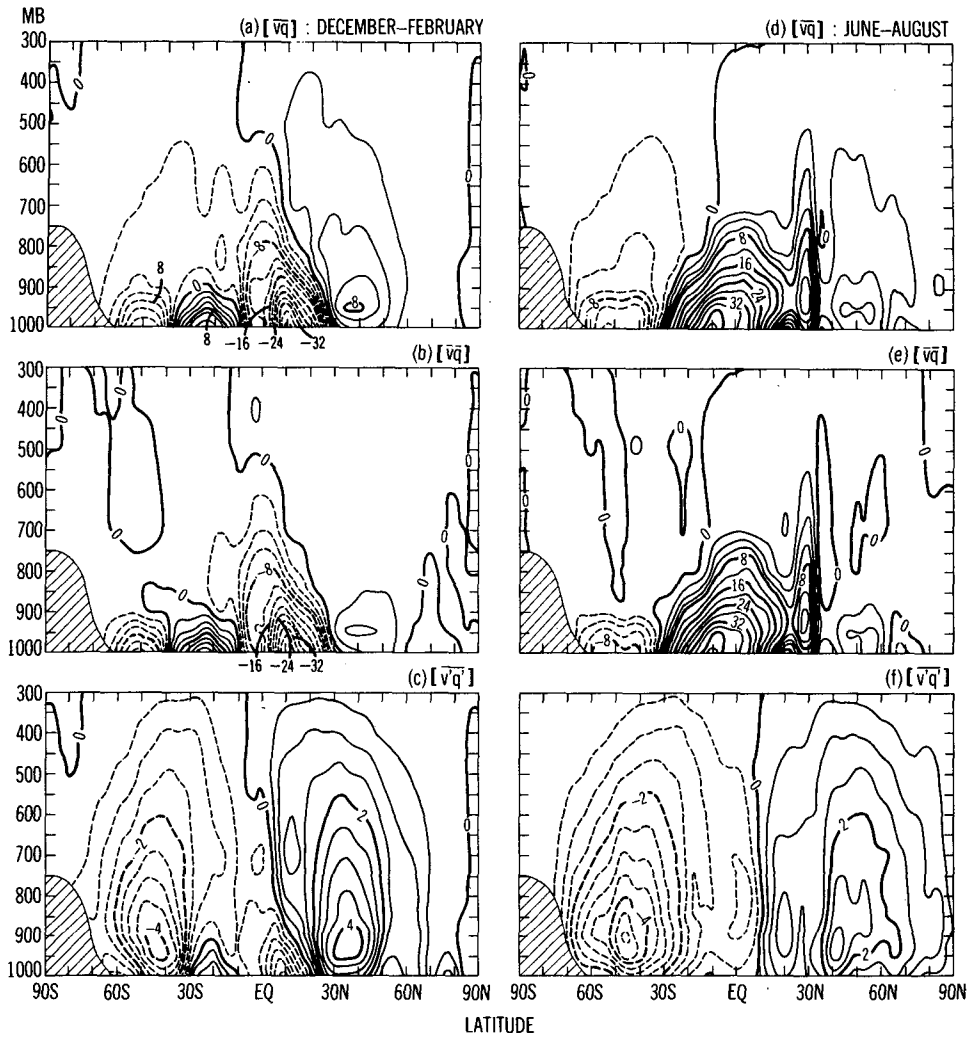

FIG. 6. As in Fig. 4, except for the meridional flux of water vapor. The northward and southward transports are denoted by solid and dashed lines, respectively.

Gulf of Alaska and from eastern North America to south of Greenland. In the northern winter, another significant area of Q' extends from the east Atlantic to eastern Europe.

Based on IGY data analysis, Taljaard (1967) found that in the Southern Hemisphere the cyclone paths originate in the northeastern South Pacific and along the Brazilian coast. The former stretches to the South Pacific along the SPCZ, while the latter spirals in a southeasterly direction to the east Antarctic coastline of the Indian Ocean. The satellite observations of cloud bands by Hurbert *et al.* (1969), and Sadler (1970) confirm Taljaard's result. Employing a band pass filter for the 2.5–6 day period range, Physick (1981) and Trenberth (1981; 1982) showed four favored cyclogenesis regions for winter; the eastern Indian Ocean and south of Australia, the mid-Pacific Ocean, the western Atlantic Ocean of the South American coast, and south of the African continent. The areas of significant water vapor transport by the transient mode in the Southern Hemisphere (Figs. 8c and 9c) coincide with the regions of intense cyclone activity. It may be concluded that the poleward water vapor transport by the transient mode in midlatitudes of both hemispheres is accomplished essentially by the transient cyclone systems.

5. Streamfunction (ψ) and potential (χ)

The relationship between the atmospheric circulation and the water vapor transport can be illustrated by means of the streamfunction (Rosen *et al.*, 1979b) and potential (Salstein *et al.*, 1980). The large-scale atmospheric circulation is essentially nondivergent, as shown by Chen and Wiin-Nielsen (1976). It is not surprising that the large-scale atmospheric water vapor transport is largely described by the nondivergent

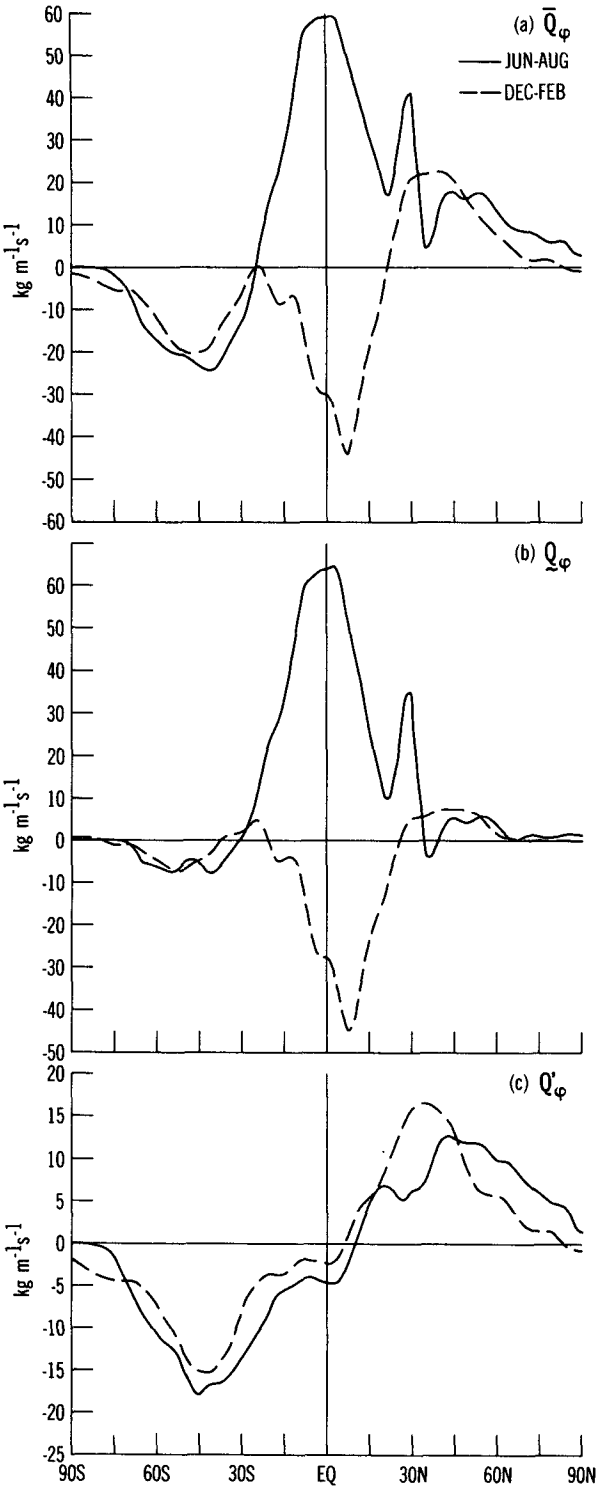

FIG. 7. As in Fig. 5, except for the meridional flux.

component, as delineated by Rosen *et al.* The streamfunction of water vapor flux can aid in visualizing the transport pattern and intensity variation.

The potential field is obtained by solving the Poisson equation using the convergence of water vapor transport flux ($\nabla \cdot \mathbf{Q}$) as forcing. The $\nabla \cdot \mathbf{Q}$ is related to the source and sink of water vapor through the water balance equation

$$\frac{\partial W}{\partial t} + \nabla \cdot \mathbf{Q} = E - P. \tag{8}$$

If this equation is averaged over a long period, such as a season, $\partial \bar{W}/\partial t$ becomes negligible, compared to other terms. Therefore, the difference between the evaporation (E) and precipitation (P) over a season can be evaluated approximately by the divergence of horizontal water vapor flux,

$$\nabla \cdot \bar{\mathbf{Q}} \approx \bar{E} - \bar{P}. \tag{9}$$

If the potential of water vapor flux is employed, we may express the time-averaged water balance equation as

$$\nabla^2 \bar{\chi} \approx \bar{E} - \bar{P}. \tag{10}$$

This equation shows that the divergent component of the water vapor flux is important to the hydrological cycle. Furthermore, the diabatic heating due to the radiation and latent heat release is related to E and P.

Section 4 indicates that the stationary (seasonal mean) mode is very representative of the total water vapor flux (Figs. 7 and 8); i.e., $\bar{\mathbf{Q}} \approx \mathbf{Q}$. In the tropics, in particular, we may approximate equations (9) and (10) as,

$$\nabla \cdot \mathbf{Q} = \nabla^2 \chi \approx \bar{E} - \bar{P}. \tag{11}$$

On the other hand, the transient mode is an effective agent transporting water vapor poleward in midlatitudes to reduce the north–south gradient of water vapor content. In conjunction with the atmospheric circulation, the streamfunction and potential for the stationary and transient modes are examined to illustrate water vapor transport.

a. Stationary mode

The streamfunction of the stationary mode during the months of December through February (northern winter) (Fig. 10) exhibits a three-cell structure in the Southern Hemisphere with centers around 30°S. Each cell corresponds to the anticyclonic transport of water vapor in each ocean. The intensity of the south Indian Ocean cell is weakest. In the Northern Hemisphere, the two-cell structure of the winter season found by Peixoto *et al.* (1981) does not appear in the present study; instead a very elongated cell extends from the Atlantic to the eastern Pacific. In addition, there is a strong cell over the equatorial western Pacific which does not appear in the study by Peixoto *et al.*

In addition to the cellular pattern of the stationary streamfunction, its zonal characteristics and significant north–south gradient reflect a strong westward zonal transport in the tropics and strong zonal eastward

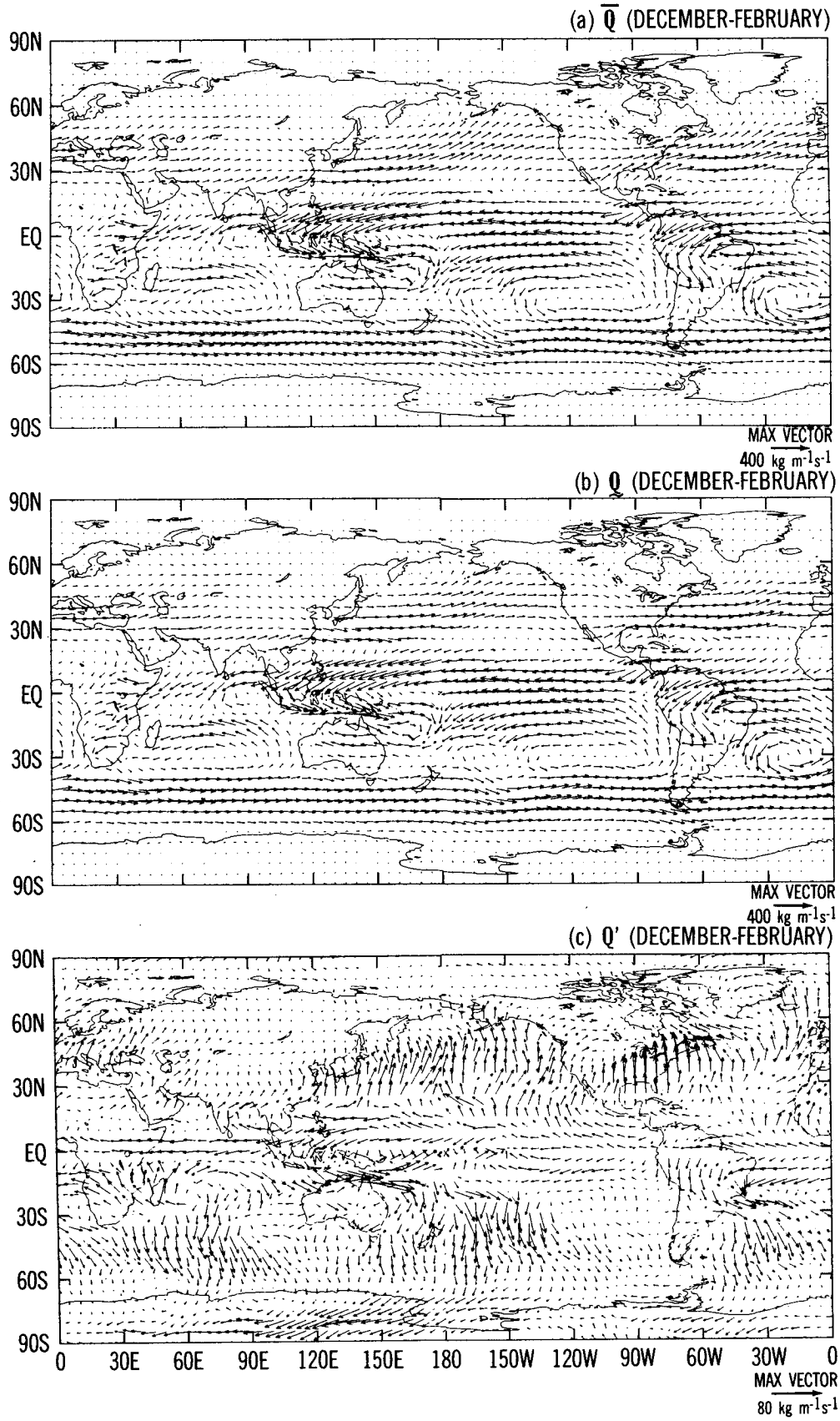

FIG. 8. Vertically integrated water vapor transport vector field of (a) the total flow $\bar{\mathbf{Q}}$; (b) the standing mode $\mathbf{Q}$; (c) the transient mode $\mathbf{Q}'$ for December–February. Vector units: kg m^{-1} s^{-1}.

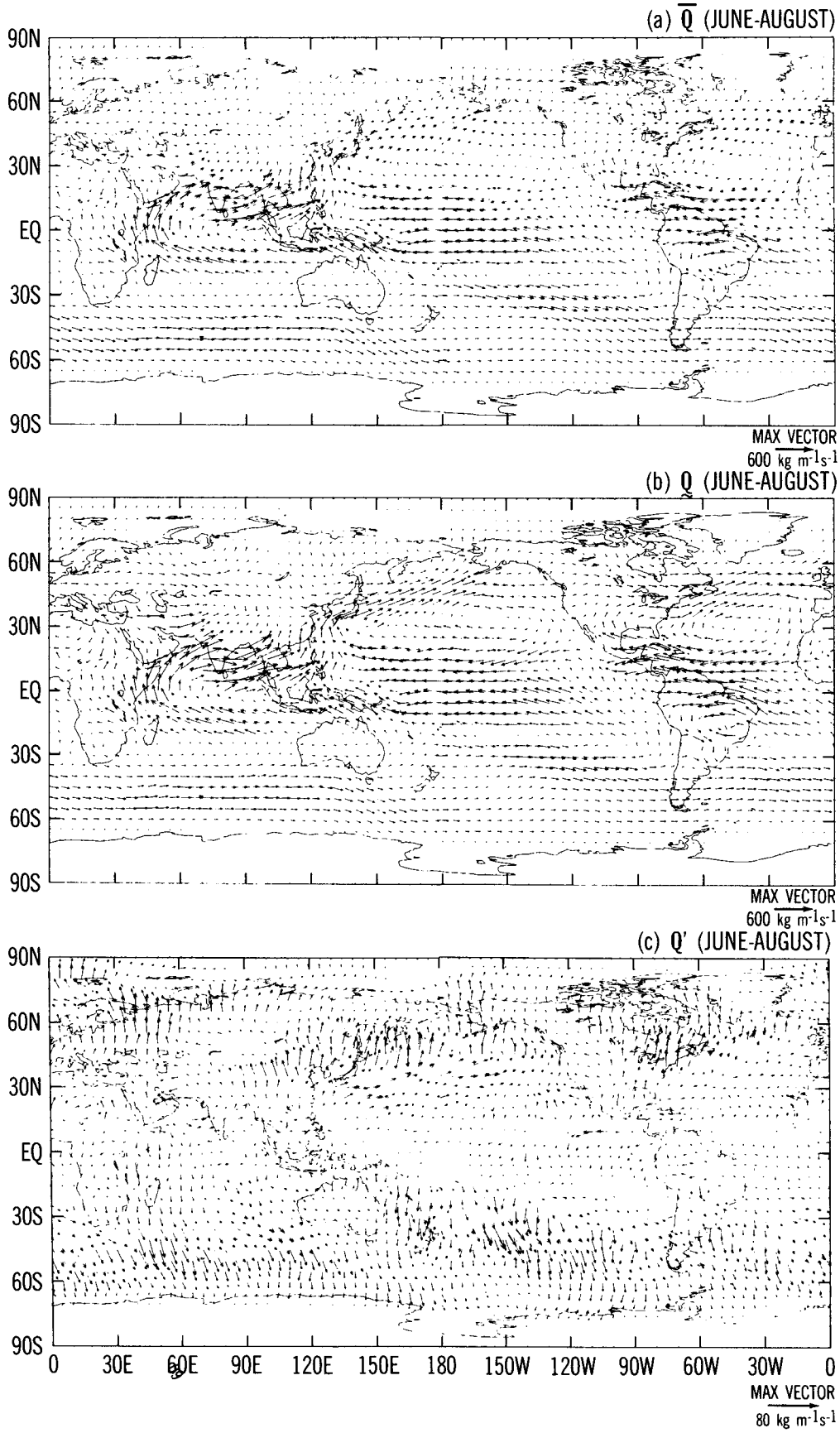

FIG. 9. As in Fig. 8, except for June–August.

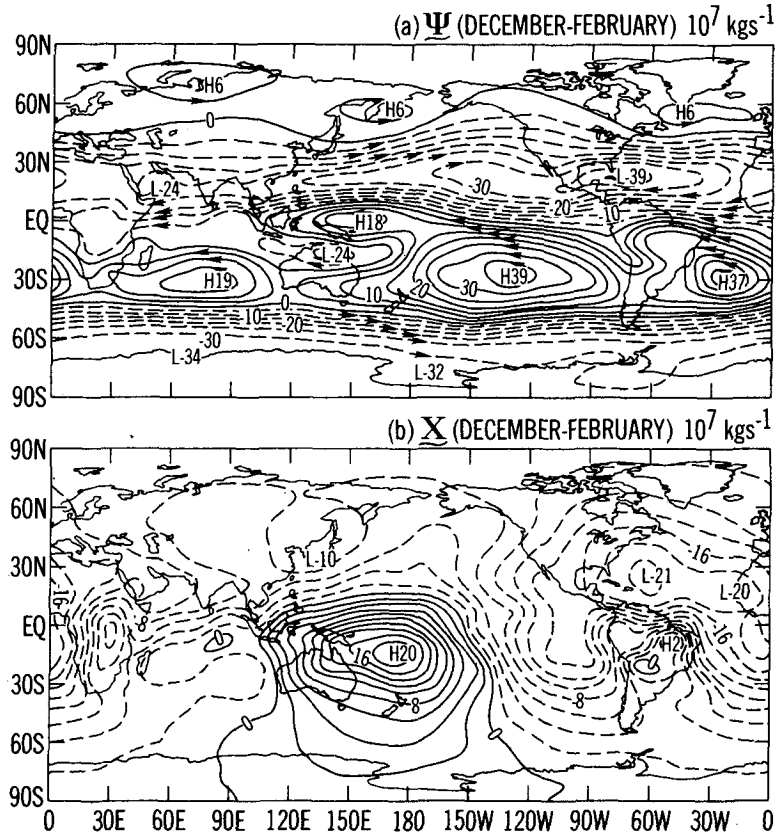

FIG. 10. Global distribution of (a) streamfunction (ψ) and (b) potential (χ) for the vertically integrated water vapor flux of the standing mode during December–February. Unit: 10^7 kg s^{-1}.

transport in the midlatitudes of both hemispheres. The disappearance of the Pacific cell indicates that the northward transport in the western Pacific and the southward transport in the eastern Pacific around the horse latitudes are much weaker than the results of Peixoto *et al.*

In June–August (Fig. 11), the South Indian Ocean cell disappears. The intensity of both the Pacific and Atlantic cells in the Southern Hemisphere becomes comparable and also moves somewhat more northward toward the equator than in the southern summer season (December–February). Since the water vapor content decreases in the winter season, the increase in intensity of these two cells may be attributed to the intensification of the low-level tropical circulation in the two oceans. The disappearance of the south Indian Ocean cell is because of a pronounced seasonal variation there due to the direction change between the winter and summer monsoon. A three-cell structure becomes very evident in the Northern Hemisphere with the center of each cell over the Pacific, Atlantic, and monsoon areas. The winter–summer contrast in cell intensity is greater in the Northern Hemisphere. The strong zonal westward and eastward transport still exists in the tropics and Southern Hemisphere, respectively, in this season. Conversely, the eastward transport in the midlatitudes of the Northern Hemisphere becomes segmental because of the cellular structure. It is interesting that the nondivergent component of water vapor transport over equatorial Africa is negligible.

It is evident from the comparison between Figs. 8 and 9 and also Figs. 10 and 11 that the streamfunction field of the stationary mode is similar to the total water vapor transport $\bar{\mathbf{Q}}$ and the water vapor transport of stationary mode $\mathbf{Q}$. Furthermore, it will be shown later that the magnitude of the potential field is so much smaller than that of the streamfunction field that the nondivergent component of the stationary mode is representative of the total water vapor transport, as Rosen *et al.* (1979b) and Peixoto *et al.* (1981) argued.

Analysis of the streamfunction does not answer the question of how the high water vapor content of several specific areas is maintained. Therefore, let us turn our attention to the potential field. According to the approximate water balance equation (11), the Laplacian of standing potential (χ) is approximately equivalent to the source or sink of water vapor ($\bar{E} - \bar{P}$). The potentials of stationary-mode water vapor flux (χ) for December through February and June through August are displayed in Figs. 10b and 11b, respectively.

The $\bar{\chi}$ field of the present study for each individual season is different from the yearly mean $\bar{\chi}$ field of Sal-

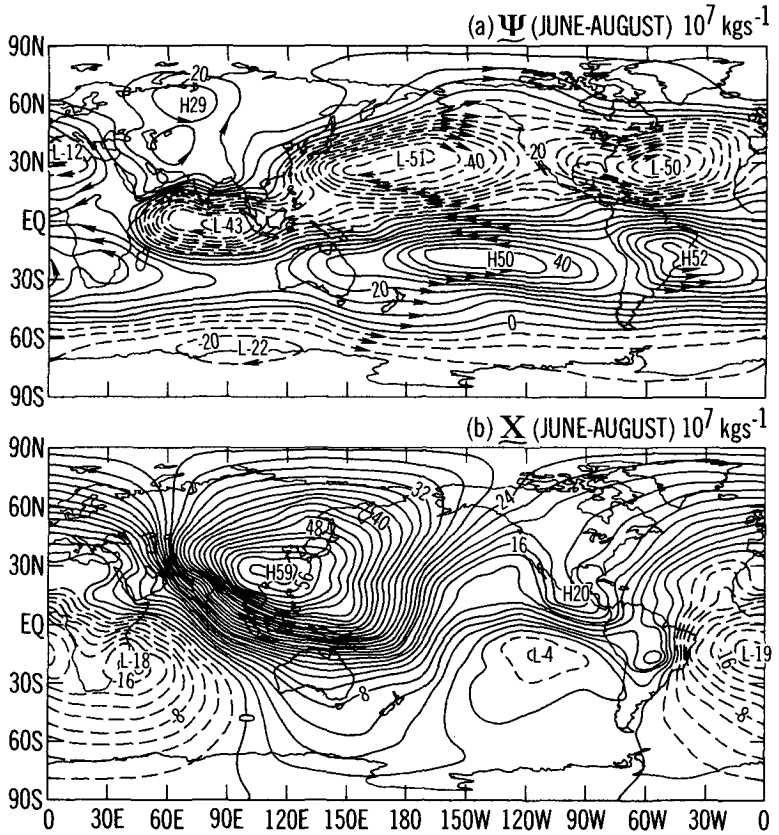

FIG. 11. As in Fig. 10, except for June–August.

stein *et al.* However, the average of our summer and winter χ field is similar to theirs except that their negative center of χ at 15°N is north of the result of this work. The northward shift of Salstein's negative $\bar{\chi}$ center may be due to the boundary of their computational domain which is too close to these centers.

The magnitude of χ is smaller than that of ψ, implying as previously noted, that the divergent component of the stationary-mode water vapor flux is smaller than the nondivergent component. In June through August, the magnitude of χ is enhanced very significantly. It is inferred that the divergent component of water vapor flux is much stronger in the northern summer season. The χ field is also more organized in this season as shown in Fig. 11b.

According to Eq. (6), the ψ field is used to illustrate the water vapor transport, but not the χ field. Instead, the gradient of the χ field, $\nabla\chi$, provides the divergent components of the standing water vapor flux. The vector plots of $\nabla\chi$ for both seasons are displayed in Fig. 12. Note that various cells of the χ field juxtapose each other. The zonal and meridional components of the divergent water vapor flux are comparable in contrast to the dominance of zonal component in the nondivergent water vapor flux. It has been indicated by earlier studies (Rasmusson, 1972) that the zonally-averaged meridional transport of water vapor in the tropics is accomplished by the lower branch of Hadley circulation. Salstein *et al.* (1980) suggest that the zonal component of the divergent water vapor flux is related to the Walker circulation. The configuration of the stationary-mode divergent water vapor flux exhibited in Fig. 12 in the zonal direction is consistent with the lower branch of the Walker circulation shown by Webster (1983, Fig. 9.4).

At this point, it is of interest to compare the convergence of water vapor flux by the stationary divergent mode (Fig. 12) and the geographic distribution of $\bar{W}$ (Fig. 3). Observations reveal that the water vapor converges toward three tropical areas of high water vapor content and seems to indicate that the local Hadley circulation and the longitudinal Walker circulation perform the water vapor transport to maintain the high water vapor content over three preferable tropical areas. The converged water vapor would be transported upward by the two types of circulations to increase the moisture content of the atmosphere and, in turn, to enhance the condensation. If our reasoning is right, the large rainfall in the tropics should be consistently distributed with the significant convergence of water vapor flux.

According to the time-averaged water balance equation, it may be expected that the source (sink) of water vapor, $\bar{E} - \bar{P}(\approx \nabla \cdot \mathbf{Q}_\chi) < 0 (\bar{E} - \bar{P} \approx \nabla \cdot \mathbf{Q}_\chi > 0)$

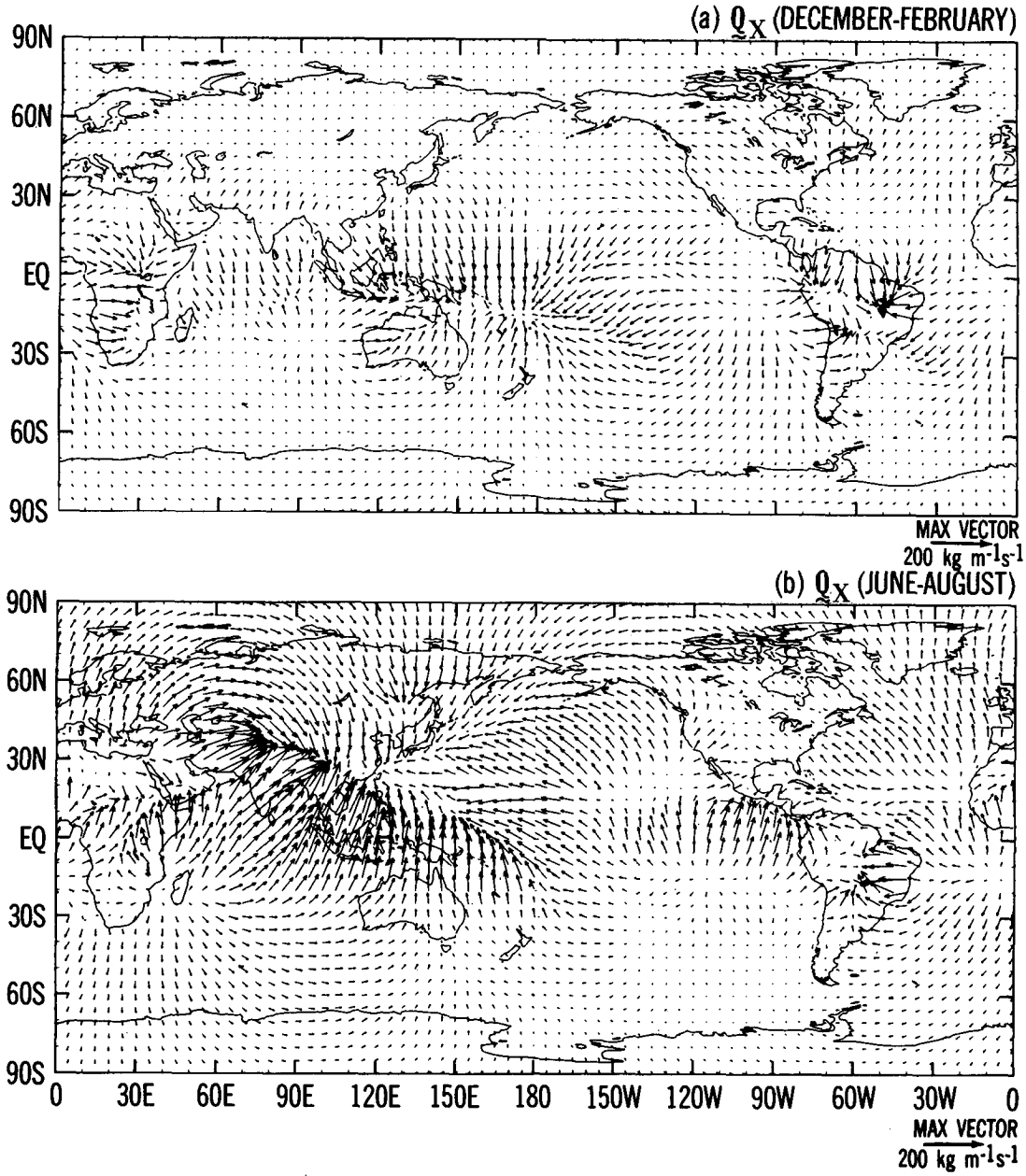

FIG. 12. Divergent component of the vertically integrated standing water vapor transport vector field for: (a) December–February; and (b) June–August. Vector units: kg m^{-1} s^{-1}.

goes hand in hand with the convergence (divergence) of water vapor flux. This does not necessarily mean that the high water vapor content should be associated with the large rainfall or with the convergence of water vapor flux, however. In other words, one may argue that the large evaporation rate also can increase the atmospheric water vapor content. The global evaporation rate computed by Budyko (1963) and tabulated by Schutz and Gates (1972a,b) always shows low values over those tropical areas of high water vapor content. Cornejo-Garrido and Stone (1977) have examined the heat balance of the Walker circulation, concluding that the local evaporation is negligible compared with rainfall over the equatorial Western Pacific, where the upward branch of Walker and local Hadley circulation are located. The foregoing discussion strongly indicates that the high water vapor content over three tropical areas is maintained by the convergence of the water vapor flux by the Walker circulation in the longitudinal direction and by the local Hadley circulation in the meridional circulation.

Chervin and Druyan (1984) and Stone and Chervin (1984) used the GISS model I (Hansen *et al.*, 1983) to study forcing mechanisms for the global Walker cir-

culation. They found that continentality and gradients of ocean surface temperatures, especially the former, are the major asymmetric forces responsible for the stimulation of the vertical motion of both the Walker circulation and the Hadley circulation. The generated rising motion causes the convergence of moisture and condensation, and the resulting heating due to the release of latent heat reinforces the rising motion, i.e., the intensity of the Walker and Hadley circulation. These numerical studies of the Walker circulation support the argument that the high water vapor content of three tropical areas is maintained by the Walker and local Hadley circulation.

b. Transient mode

The streamfunction of the transient water vapor flux ψ' is shown in Figs. 13a and 14a for both seasons of December–February and June–August, respectively. The ψ' is at least an order of magnitude smaller than the streamfunction of the standing water vapor flux ψ. In December–February, most of the positive and negative centers of the ψ' cells were located between the midlatitudes of both hemispheres. For instance, three positive ψ' cells corresponding to those ψ cells appear over the south Atlantic and Pacific in the Southern Hemisphere and the equatorial western Pacific (Fig. 13a). A negative cell corresponds to the positive ψ cell over the Indian Ocean. Furthermore, a weak positive ψ' cell is located over northeastern Asia. In addition, some negative ψ' centers are located in the tropics. In June–August, ψ' is cellular in the tropical areas of both hemispheres and zonal in the midlatitudes of the Southern Hemisphere. Although several ψ' centers were located in the tropics, the large ψ' centers were in higher latitudes.

Since the magnitude of ψ' is much smaller than ψ, ψ' can be regarded as the difference between $\bar{\psi}$ and ψ, which is a difference between two large quantities. The noise level of ψ' is comparable to the magnitude of ψ' itself; therefore, the physical interpretation of ψ' is by no means definitive.

The potential of the transient water vapor flux χ' for both December–February and June–August is delineated in Figs. 13b and 14b, respectively. The magnitude of χ' is smaller than χ, but much larger than ψ'. The contrast in the magnitude of χ' and ψ' implies that the water vapor flux of the transient mode is mostly described by the divergent component. Also, note that the ψ' field is cellular while the χ' field is zonal; the opposite is true in the ψ and χ field. For both seasons of this study, the minimum χ' appears in the tropics and the maximum χ' exists in the polar areas. Since the divergent component is directed from small to large

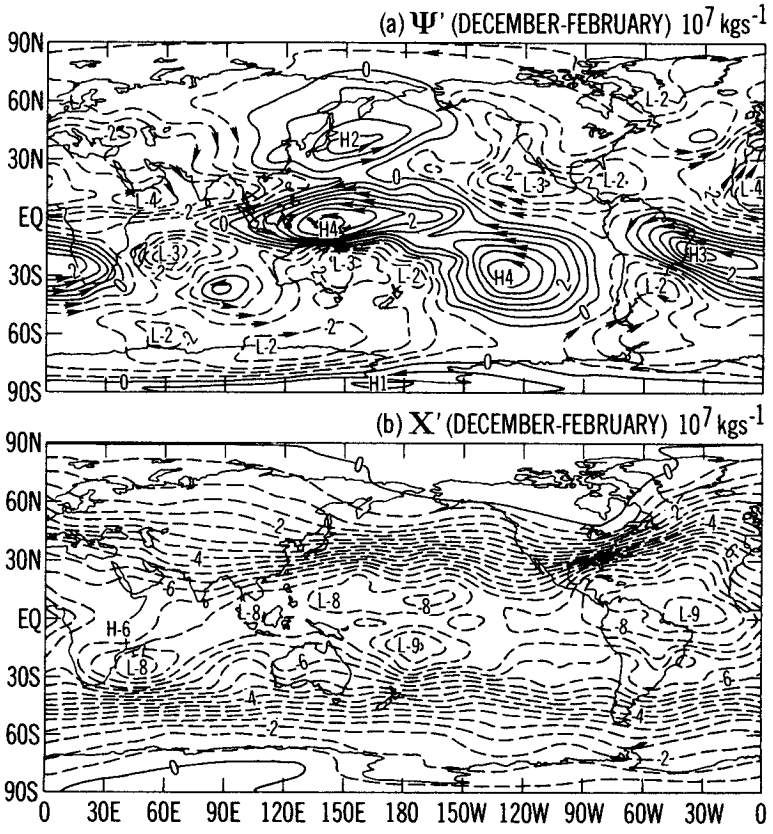

FIG. 13. As in Fig. 10, except for the transient mode during December–February.

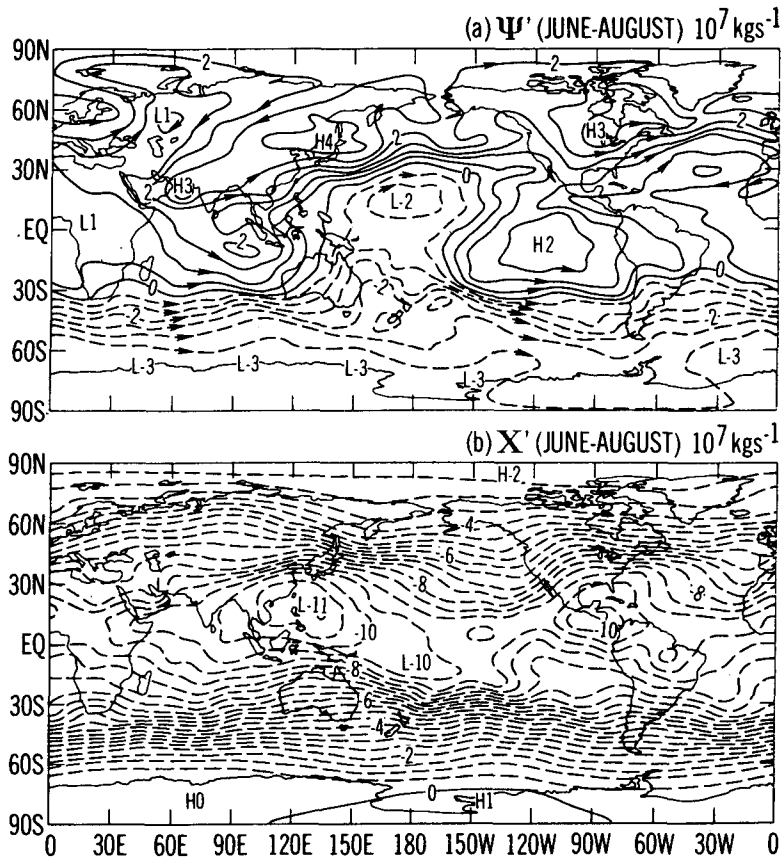

FIG. 14. As in Fig. 10 except for the transient mode during June–August.

values and the north–south gradient of χ' field is largest in the midlatitudes, it may be concluded that the poleward transport of water vapor by the transient mode in the midlatitude is largely carried out by the transient divergent component. This conclusion is based on the comparison between $\mathbf{Q}'$ (Figs. 8c and 9c) and $\mathbf{Q}'_\chi$ (Fig. 15). Furthermore, it is of interest to point out that the function of the transient mode in maintaining the water vapor source ($\bar{E} - \bar{P} < 0$) and sink ($\bar{E} - \bar{P} > 0$) is opposite to that of stationary mode.

6. Conclusions

The First Global GARP Experiment (FGGE) III-b analyses of the Geophysical Fluid Dynamics Laboratory (GFDL) are used to examine the global water vapor transport and maintenance for two extreme seasons of atmospheric circulation: December 1978–February 1979 and June 1979–August 1979. Rosen *et al.* (1985) cautioned that the moisture and transient eddy transport of water vapor at 850 mb are noisy. However, the moisture and wind fields generated at 900 and 950 mb by this analysis, in addition to conventional mandatory levels, provide major advantages for this water vapor budget analysis. The moisture budget obtained in this study is generally consistent with previous studies, with some minor discrepancies. These discrepancies might be due to differences in the data analysis and interannual variability.

For these two FGGE seasons, it was found that the stationary nondivergent mode describes most of the total water vapor transport. The stationary divergent mode, which is composed of the local Hadley circulation in the meridional direction and the Walker circulation in the zonal direction, is responsible for the maintenance of the high water vapor content over equatorial Africa, the northern part of South America, and the equatorial western Pacific during the northern winter, and equatorial Africa, Central America and the northern part of South America, and monsoon areas during the northern summer. Moreover, the transient divergent mode, which mainly is attributed to the cyclone systems in midlatitudes of both hemispheres, carries out an important part of poleward transient water vapor transport along the storm tracks and two major cloud bands in the Southern Hemisphere.

The heat budget analysis by Cornejo-Garrido and Stone (1977), the theoretical study by Geisler (1981), and the numerical circulation of the Walker circulation by Chervin and Druyan (1984) and Stone and Chervin (1984) demonstrate that the Walker circulation is generated mainly by the continentality and the gradient

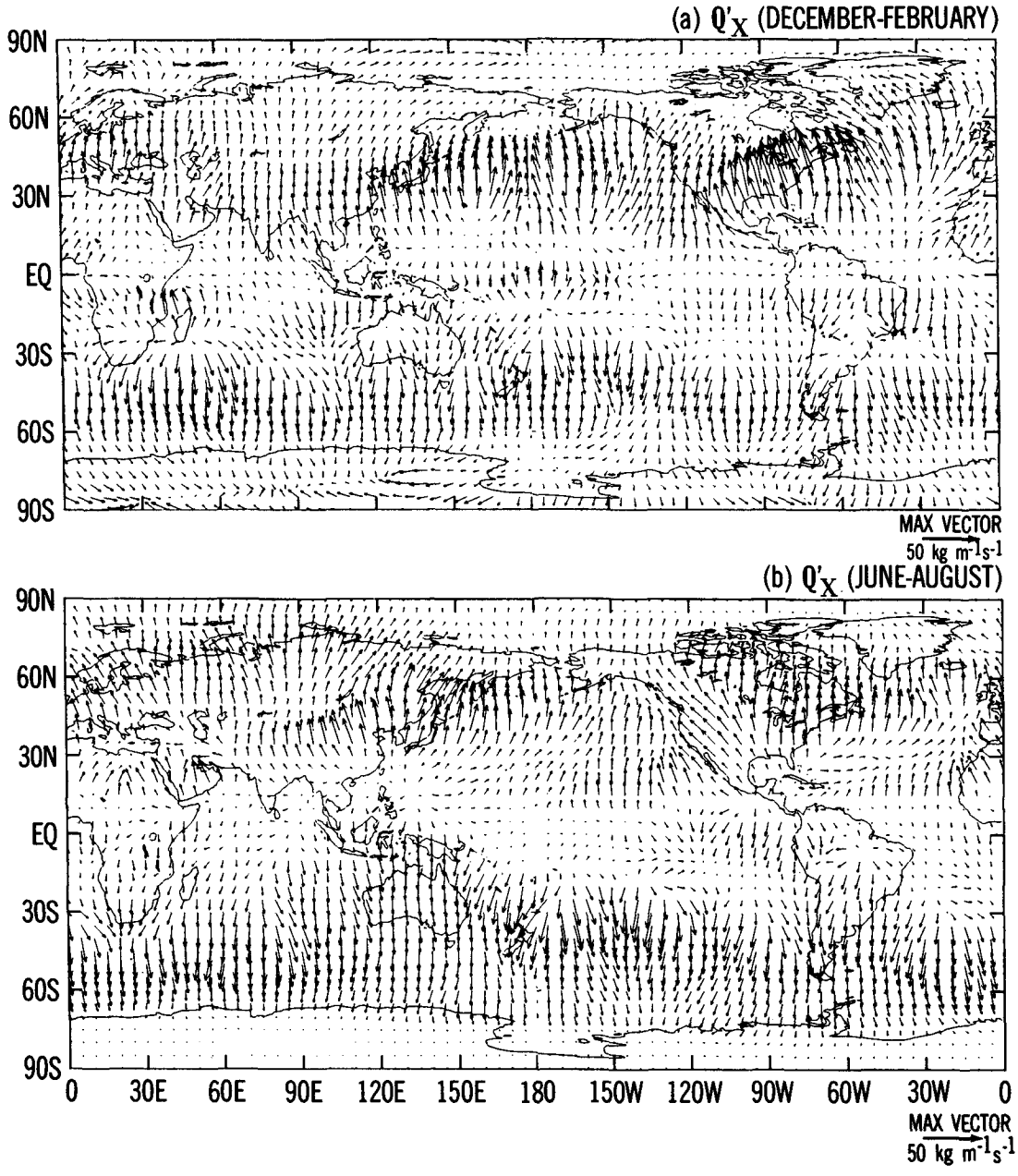

FIG. 15. As in Fig. 12, except for the divergent component of transient mode.

of ocean surface temperature in the tropics. These studies also show that the vertical motions associated with the Walker circulation converge the water vapor and transport it upward to maintain the high water vapor content over three tropical areas where the upward branches of the Walker and local Hadley circulation exist.

It was illustrated by Bjerknes (1969) that the interannual variation of the intensity of the Walker circulation is in phase with the Southern Oscillation. Stoecknius (1981) suggested that the intensity variation of the Walker circulation, instead of the Hadley circulation, accounts for most of the observed interannual rainfall variation. According to the water balance equation, the interannual rainfall variation is directly related to the water vapor transport by the stationary divergent mode in the tropics. Therefore, the interannual variation on the zonal water vapor flux of the stationary divergent mode should be synchronized with the Southern Oscillation. This is one interesting aspect of tropical climatology which must be pursued in further research.

Acknowledgments. This study is supported jointly by the National Science Foundation and the National Oceanic and Atmospheric Administration under Grants ATM-8206798 and NA82AA-0-00035. The computations of this study were performed with the computing facility of the National Center for Atmospheric Research which is sponsored by the National Science Foundation. Suggestions made by Drs. Richard D. Rosen and David A. Salstein have been helpful in clarifying some critical aspects of this paper. Conversation with Dr. J. Ploshay explained some issues regarding the FGGE III-b moisture analysis of the Geophysical Fluid Dynamics Laboratory. The encouragement provided by Dr. K. Miyakoda and comments by Dr. K. E. Trenberth, Mr. R. H. Langland and reviewers are helpful in improving this paper. I also wish to thank Drs. Jordan C. Alpert and Douglas N. Yarger for their editorial comments.

REFERENCES

Benton, G. S., and M. A. Estogue, 1954: Water vapor transfer over the North American continent. *J. Meteor.*, **11,** 462–477.

Bjerknes, J., 1969: Atmospheric teleconnection from the equatorial Pacific. *Mon. Wea. Rev.*, **97,** 163–172.

Blackmon, M. L., 1976: A climatological spectral study of the 500 mb geopotential height of the Northern Hemisphere. *J. Atmos. Sci.*, **33,** 1607–1623.

Budyko, M. I., 1963: *Atlas of the Heat Balance of the Earth, Gidrometeor.*, 5 pp., 69 maps.

Chen, T.-C., and A. Wiin-Nielsen, 1976: On the kinetic energy of divergent and nondivergent flow in the atmosphere. *Tellus,* **28,** 486–498.

——, C. B. Chang and D. J. Perkey, 1985: Synoptic study of a medium-scale oceanic cyclone during AMTEX '75. *Mon. Wea. Rev.*, **113,** 349–361.

Chervin, R. M., and L. M. Druyan, 1984: The influence of ocean surface temperature gradient and continentality on the Walker circulation. Part I: Prescribed tropical changes. *Mon. Wea. Rev.*, **112,** 1510–1523.

Cornejo-Garrido, A. G., and P. H. Stone, 1977: On the heat balance of the Walker circulation. *J. Atmos. Sci.*, **34,** 1155–1162.

Geisler, J. E., 1981: A linear model of Walker circulation. *J. Atmos. Sci.*, **38,** 1390–1400.

Goff, J. A., and S. Gratch, 1946: Low-pressure properties of water from −160 to 212°F. *Trans. Amer. Soc. Heat and Vent. Eng.*, **52,** 95–122.

Greenfield, R. S., and T. N. Krishnamurti, 1979: The winter monsoon experiment. Report of the December 1978 field phase. *Bull. Amer. Meteor.*, **60,** 439–444.

Hansen, J., G. Russell, D. Rind, P. Stone, A. Lacis, S. Lebedff, R. Ruedy and L. Travis, 1983: Efficient three-dimensional global models for climate studies: Models I and II. *Mon. Wea. Rev.*, **111,** 609–662.

Howarth, D. A., 1983: Seasonal variations in the vertically integrated water vapor transport fields over the Southern Hemisphere. *Mon. Wea. Rev.*, **111,** 1259–1272.

Hurbert, L. F. A., A. F. Krueger and J. S. Winston, 1969: The double intertropical convergence zone—fact or fiction? *J. Atmos. Sci.*, **26,** 771–773.

James, I. N., and D. L. T. Anderson, 1984: The seasonal mean flow and distribution of large-scale weather systems in the Southern Hemisphere: The effects of moisture transports. *Quart. J. Roy. Meteor. Soc.*, **110,** 943–966.

Julian, P. R., 1984: Some comparison of ECMWF III-b and GFDL III-b analyses in the tropics. *Global Weather Experiment Newsletter, No. 3,* USC-GARP, National Academy of Sciences, Washington, DC, 20–22.

Lau, K.-M., and P. H. Chan, 1983: Short-term climate variability and atmospheric teleconnections from satellite-observed outgoing longwave radiation. Part I: Simultaneous relationship. *J. Atmos. Sci.*, **40,** 2735–2750.

Liebman, B., and Hartman, D. L., 1981: Interannual variation of outgoing IR association with tropical circulation changes during 1974–78. *J. Atmos. Sci.*, **28,** 1153–1162.

Miyakoda, K., J. Sheldon and J. Sirutis, 1982: Four-dimensional analysis experiment during the GATE period. Part II. *J. Atmos. Sci.*, **39,** 486–506.

Peixoto, J. P., 1970: Pole-to-pole divergence of water vapor. *Tellus,* **22,** 17–25.

——, and A. H. Oort, 1983: The atmospheric branch of the hydrological cycle and climate, *Variation in the Global Water Budget,* A. Street-Perrott *et al.*, Ed. Reidel, 5–65.

——, R. D. Rosen and D. A. Salstein, 1978: Seasonal variability in the pole-to-pole modes of water vapor transport during the IGY. *Arch. Met. Geoph. Biokl.*, **A27,** 233–255.

——, D. A. Salstein and R. D. Rosen, 1981: Intra-annual variation in large-scale moisture fields. *J. Geophys. Res.*, **86,** 1255–1264.

Physick, W. L., 1981: Winter depression tracks and climatologist jet streams in the Southern Hemisphere during the FGGE year. *Quart. J. Roy Meteor. Soc.*, **107,** 883–898.

Ploshay, J., R. White and K. Miyakoda, 1983a: FGGE III-b daily global analyses—Part I. *NOAA Data Report, ERL GFDL-1,* GFDL, Princeton, NJ.

——, —— and ——, 1983b: FGGE III-b daily global analysis—Part III. *NOAA Data Report, ERL GFDL-1,* GFDL, Princeton, NJ.

Rasmusson, E. M., 1972: Seasonal variation of tropical humidity parameters. *The General Circulation of the Tropical Atmosphere and Interactions with Extratropical Latitudes,* Vol. I, MIT Press.

Rosen, R. D., D. A. Salstein and J. P. Peixoto, 1979a: Variability in the annual fields of large-scale atmospheric water vapor transport. *Mon. Wea. Rev.*, **107,** 26–37.

——, —— and ——, 1979b: Streamfunction analysis of inter-annual variability in large-scale water vapor flux. *Mon. Wea. Rev.*, **107,** 1682–1684.

——, ——, ——, A. H. Oort and N.-G. Lau, 1985: Circulation statistics derived from level III-b and station-based analyses during FGGE. *Mon. Wea. Rev.*, **113,** 65–88.

Sadler, J. C., 1970: Mean cloudiness and gradient level wind chart over the tropics. Air Weather Service Technical Report 215, Vol. II, 60 pp.

Salstein, D. A., R. D. Rosen and J. P. Peixoto, 1980: Hemispheric water vapor flux variability—streamfunction and potential fields. *Atmospheric Water Vapor,* A. Deepak, T. D. Wilkerson and L. H. Ruhnke Eds., Academic Press, 1980, 557–574.

——, —— and ——, 1983: Modes of variability in annual hemispheric water vapor and transport fields. *J. Atmos. Sci.*, **40,** 788–803.

Schutz, C., and W. Gates, 1972a: Global climatic data for surface, 800 mb, 400 mb: July. Rep. R-1029-ARPA, The Rand Corporation, 1700 Main St., Santa Monica, Calif. 90406.

——, and ——, 1972b: Global climatic data for surface, 800 mb, 400 mb. Rep. R-1029-ARPA, The Rand Corporation, 1700 Main St., Santa Monica, Calif. 90406.

Sirutis, J., K. Miyakoda and J. Ploshay, 1980: Moisture distribution derived in mathematical models and four-dimensional analysis. *Atmospheric Water Vapor,* Ed. A. Deepak, T. D. Wilkerson and L. H. Rukne Eds., Academic Press, 1980, 489–496.

Starr, V. P., and R. M. White, 1955: Direct measurement of the hemispheric poleward flux of water vapor. *J. Mar. Res.*, **14,** 217–225.

——, and J. P. Peixoto, 1958: On the global balance of water vapor and the hydrology of deserts. *Tellus,* **10,** 188–194.
——, and ——, 1964: The hemispheric eddy flux of water vapor and its implications for the mechanics of the general circulation. *Arch. Meteor. Geoph. Biokl.,* Ser. A., **14,** 111–130.
——, and ——, 1971: Pole-to-pole eddy transport of water vapor in the atmosphere during the IGY. *Arch. Meteor. Geoph. Biokl.,* Ser. A, **20,** 85–114.
——, and B. Saltzman, 1966: Observational studies of the atmospheric general circulation. Scientific Rep. No. 2, Planetary Circulation Project, Dept. of Meteorology, MIT, Cambridge, Mass. 02108.
——, J. P. Peixoto and G. C. Livadas, 1958: On the meridional flux of water vapor in the Northern Hemisphere. *Geof. Pura. e Appl.,* **39,** 174–185.
Stoeckenius, T., 1981: Interannual variations of tropical precipitation patterns. *Mon. Wea. Rev.,* **109,** 1233–1247.
——, —— and A. R. Crisi, 1965: Hemispheric water balance for the IGY. *Tellus,* **17,** 463–472.
Stone, P. H., and R. M. Chervin, 1984: The influence of ocean surface temperature gradient and continentality of the Walker circulation. Part II. Prescribed global changes. *Mon. Wea. Rev.,* **112,** 1524–1534.
Swarztrauber, P. N., 1974: The direct solution of the discrete Poisson equation on the surface of a sphere. *Comput. Phys.,* **15,** 46–54.
Taljaard, J. J., 1967: Development, distribution and movement of cyclones and anticyclones in the Southern Hemisphere during the IGY. *J. Appl. Meteor.,* **6,** 973–987.
Trenberth, K. E., 1981a: Observed Southern Hemisphere eddy statistics at 500 mb: Frequency and spatial dependence. *J. Atmos. Sci.,* **38,** 2585–2605.
——, 1981b: Seasonal variations in global sea level pressure and the total mass of the atmosphere. *J. Geophys. Res.,* **86,** 5236–5246.
——, Seasonality in Southern Hemisphere eddy statistics at 500 mb. *J. Atmos. Sci.,* **39,** 2507–2520.
Viswanadham, Y., N. J. M. Rao and G. S. S. Nunes, 1980: Some studies on moisture conditions in the Southern Hemisphere. *Tellus,* **32,** 131–142.
Webster, P. J., 1983: The large-scale structure of the tropical atmosphere, *Large-Scale Dynamical Processes in the Atmosphere,* B. J. Hoskins and R. P. Pearce, Eds., Academic Press, 235–275.